minerals

MDPI

Article

Capacity of Chlorate to Oxidize Ferrous Iron: Implications for Iron Oxide Formation on Mars

Kaushik Mitra [1], Eleanor L. Moreland [1] and Jeffrey G. Catalano [1,2,*]

[1] Department of Earth & Planetary Sciences, Washington University, St. Louis, MO 63130, USA; k.mitra@wustl.edu (K.M.); morelandellie@wustl.edu (E.L.M.)

[2] McDonnell Center for the Space Sciences, Washington University, St. Louis, MO 63130, USA

* Correspondence: catalano@wustl.edu

Received: 20 July 2020; Accepted: 17 August 2020; Published: 19 August 2020

Abstract: Chlorate is an important Cl-bearing species and a strong potential Fe(II) oxidant on Mars. Since the amount of oxychlorine species (perchlorate and chlorate) detected on Mars is limited (<~1 wt.%), the effectiveness of chlorate to produce iron oxides depends heavily on its oxidizing capacity. Decomposition of chlorate or intermediates produced during its reduction, before reaction with Fe(II) would decrease its effective capacity as an oxidant. We thus evaluated the capacity of chlorate to produce Fe(III) minerals in Mars-relevant fluids, via oxidation of dissolved Fe(II). Each chlorate ion can oxidize 6 Fe(II) ions under all conditions investigated. Mass balance demonstrated that 1 wt.% chlorate (as ClO_3^-) could produce approximately 6 to 12 wt.% Fe(III) or mixed valent mineral products, with the amount varying with the formula of the precipitating phase. The mineral products are primarily determined by the fluid type (chloride- or sulfate-rich), the solution pH, and the rate of Fe(II) oxidation. The pH at the time of initial mineral nucleation and the amount of residual dissolved Fe(II) in the system exert important additional controls on the final mineralogy. Subsequent diagenetic transformation of these phases would yield 5.7 wt.% hematite per wt.% of chlorate reacted, providing a quantitative constraint on the capacity of chlorate to generate iron oxides on Mars.

Keywords: Mars; oxychlorine; iron oxides; chlorate; oxidation

1. Introduction

The dominant reddish hue characteristic of Mars is caused by the distribution of various Fe(III)-oxides and oxyhydroxides on its surface. Several Fe(III)-bearing minerals were identified in numerous rocks, soils, sediments, and meteorite samples of Mars, including hematite [α-Fe_2O_3] [1–7], goethite [α-FeOOH] [5,8], akaganeite [β-FeO(OH,Cl)] [9,10], lepidocrocite [γ-FeOOH] [11], jarosite [$(K,Na,H_3O)Fe_3(OH)_6(SO_4)_2$] [4,6,7,12–16], and schwertmannite [$\sim Fe_8O_8(OH)_6SO_4$] [17]. The mixed valent iron oxide magnetite [Fe_3O_4] was also found on Mars [5,9,18–21]. Although hematite is thermodynamically the most stable Fe(III)-oxide mineral [22], its direct precipitation by oxidation of dissolved Fe(II) is kinetically inhibited at low-temperatures (<~70 °C) [23]. Phase transformations of other iron oxides and oxyhydroxides can produce hematite [24–32] through various diagenetic processes [24,33–44]. Formation of metastable, precursor Fe(III) oxides and oxyhydroxides, through oxidation of dissolved Fe(II) was studied for a variety of oxidants, including O_2, UV light, and hydrogen peroxide [45–48]. A recent study [49] demonstrated the potential for chlorate (ClO_3^-), an important oxychlorine species on Mars, to oxidize dissolved Fe(II) under Mars-relevant conditions and produce Fe(III)-bearing minerals.

Oxychlorine [chlorate and perchlorate (ClO_4^-)] salts are globally distributed and are ubiquitous on the Martian surface [50], occurring at levels of up to 1 wt.% [51]. Chlorate was identified as one of

the likely sources of evolved O_2 gas from the Rocknest (RN) [52,53], John Klein (JK), and Cumberland (CB) [51] drill samples, during high temperature pyrolysis experiments from the Sample Analysis at Mars (SAM) instrument at the Gale Crater. Laboratory studies indicate that O_2 and HCl gas releases from SAM pyrolysis experiments are most consistent with chlorate salts and chlorate salts/Fe oxides mixtures [54,55]. While chlorate was not detected at the Phoenix landing site in coexistence with perchlorate salts [56], its presence cannot be precluded, owing to the nature of the ion-selective electrode employed, which was approximately 1000 times more sensitive to perchlorate than chlorate [57]. Any chlorate present in Phoenix soil samples might therefore be masked in the presence of perchlorate [57]. Terrestrial field studies of oxychlorine salt occurrences and laboratory investigations of their formation processes indicate that chlorate should generally co-form with perchlorate in equimolar or greater proportions [58–60]. Chlorate is therefore likely to be an important Cl-bearing species that is widespread on the surface of Mars, but our knowledge of its occurrence is limited by the lack of ability to detect this species in many past landed missions. While chlorate likely always co-occurs with perchlorate, the latter displays no reactivity towards Fe(II) [49,61,62] and is not relevant to iron chemistry on the Martian surface.

Fe(II) oxidation by ClO_3^- is represented by the following net redox reaction [63–65]:

$$6Fe^{2+} + ClO_3^- + 6H^+ = 6Fe^{3+} + Cl^- + 3H_2O \quad (1)$$

According to Equation (1), each ClO_3^- ion has a maximum stoichiometric capacity to oxidize 6 Fe(II) ions to Fe(III), which can then undergo hydrolysis to produce Fe(III)-bearing minerals. Although our previous study demonstrated the kinetic potential of ClO_3^- to produce Fe(III) minerals under Mars-relevant conditions, the effective stoichiometric efficiency of each ClO_3^- ion to oxidize Fe(II) is unknown [49]. Earlier studies were conducted with a substantial stoichiometric excess of chlorate [49,63,66,67]. Notably, in Mitra and Catalano (2019), the observed ClO_3^- consumption was greater than the expected one-sixth (~16.7%), as calculated by the reaction stoichiometry. The chlorate concentration decreased by ~34% in chloride fluids and ~21% in sulfate fluids. ClO_3^- was shown to self-decompose via one or more comproportionation or disproportionation pathways, in acidic chloride-containing fluids [68], thereby reducing the effective capacity of ClO_3^- to oxidize Fe(II). In addition, ClO_3^- reduction to chloride by dissolved Fe(II) occurs sequentially through six stepwise reactions [69], generating a series of reactive, intermediate, chlorine-bearing species. The relative rates of decomposition and oxidization of Fe(II) by these species is unclear. If chlorate or its intermediate reduction products partially break down before they fully react with Fe(II), then the overall capacity for iron oxidation by chlorate is lower than the theoretical 6:1 molar ratio. While this excess chlorate consumption in our prior study might have been an analytical error [49], if valid, then the amount of Fe(II) that ClO_3^- can oxidize would be halved.

Since the amount of ClO_3^- expected to be present in Martian near-surface systems is limited (<1 wt.%, not accounting for regeneration processes [70–75]), understanding its actual capacity to oxidize dissolved Fe(II) in Mars-relevant fluids might better constrain iron oxidation processes and the resulting products. The number of moles of Fe(II) oxidized per mole of ClO_3^- ions relative to its maximum, theoretical capacity of 6:1 (Equation (1)), is referred to as the "stoichiometric efficiency". The rate of Fe(II) oxidation by chlorate is faster than by O_2 or through UV-photooxidation, by orders of magnitude in fluids similar to the Martian surface waters [49]. However, the amount of ClO_3^- in Martian soil or sediments could be an important limiting factor in determining its relative contribution as an Fe(II) oxidant on Mars. In addition, this stoichiometric efficiency potentially varies with fluid composition (e.g., chloride concentration, pH) and will be affected by the aqueous speciation of chlorine and dissolved Fe(II). Therefore, determining the stoichiometric efficiency of ClO_3^- to oxidize Fe(II) is necessary to understanding the net capacity for this oxychlorine species to oxidize dissolved Fe(II) in surface and subsurface aqueous systems on Mars.

In this study, we evaluate the stoichiometric efficiency of chlorate to oxidize Fe(II) in Mars-relevant fluids and the resultant Fe(III) minerals. The experiments were conducted at $[Fe(II)]/[ClO_3^-]$ ratios under chlorate-equivalent ($[Fe(II)]/[ClO_3^-] \approx 6$) and chlorate-deficient ($[Fe(II)]/[ClO_3^-] \approx 10:1$) conditions, to measure the maximum amount of Fe(II) oxidation by chlorate that is possible in Mars-relevant fluid compositions. The kinetics of Fe(II) oxidation were compared to our previously

proposed rate model [49], which explicitly assumed full chlorate efficiency, to compare the practical oxidation capacity of chlorate against its theoretical maximum. Our results would allow us to examine the applicability, as well as the limits of the kinetic model, in conditions that are geochemically different than those in which it was originally parameterized. The resulting mineral products were identified and quantified to determine the different iron oxides produced by chlorate as a function of fluid composition.

2. Materials and Methods

2.1. Kinetic Experiments

The maximum capacity of chlorate to oxidize dissolved Fe(II) was investigated in chlorate-equivalent and chlorate-deficient systems. The experiments were conducted using solutions prepared using ACS-grade Fisher Scientific chemicals [ferrous chloride tetrahydrate ($FeCl_2 \cdot 4H_2O$), ferrous sulfate heptahydrate ($FeSO_4 \cdot 7H_2O$), magnesium chloride hexahydrate ($MgCl_2 \cdot 6H_2O$), magnesium sulfate heptahydrate ($MgSO_4 \cdot 7H_2O$), and sodium chlorate ($NaClO_3$) and deoxygenated, deionized (DI) water. The experimental solutions were kept in aluminum foil-wrapped 50 mL polypropylene tubes, at ambient conditions (24 ± 1 °C, 1 atm), inside an anaerobic chamber (N_2 = 97%, H_2 = 3%, O_2 < 1 ppmv), to inhibit Fe(II) oxidation by unwanted oxidants. Reactors were continuously mixed on end-over-end rotators to avoid gravimetric settling of precipitates during the reaction. Chlorate-free control experiments were also prepared at pH 7 and 3 to verify the lack of inadvertent oxidation by stray oxidants (e.g., O_2) in the anaerobic chamber (Figure S1).

The reactors to study the reaction kinetics contained 40 mL solutions of ~10 mmol L^{-1} Fe(II), with either 1.67 mmol L^{-1} ClO_3^- [for Fe(II):ClO_3^- ≈ 6:1] or 1 mmol L^{-1} ClO_3^- [for Fe(II): ClO_3^- ≈ 10:1] (Table 1). An ideal chlorate-equivalent system has an initial [Fe(II)]/[ClO_3^-] that is exactly equal to 6. However, pipettor inaccuracies, dilution errors, and other experimental factors produce [Fe(II)]/[ClO_3^-] ratios that are not exactly equal to the intended ratios. Mars-relevant background salts magnesium chloride or magnesium sulfate [57,76–81] were used to serve as ionic strength buffers (~100 mmol L^{-1}) and provide anions with a different ability to complex dissolved Fe(II), affecting the reaction rates and mineral products. Owing to the similar reaction rate in chloride- and perchlorate-rich fluids [49], experiments in magnesium perchlorate fluids were not investigated to avoid redundancy. The initial pH values were set to 7, 5, or 3 using 1 mol L^{-1} hydrochloric acid and sodium hydroxide. These initial pH values were chosen to represent a range of near-neutral to acidic pH values that were thought to represent most of the fluid pH conditions on Mars [82–84]. The acidity on Mars was controlled primarily by Fe(II) oxidation and Fe(III) mineral precipitation [46], and therefore the experimental pH was allowed to drift freely as a response to Fe(II) oxidation and Fe(III) precipitation. The pH and Fe(II) concentration were measured throughout the course of the reactions, the latter via spectrophotometry, following complexation by ferrozine [85]. For dissolved Fe(II) determination by spectrophotometry, the subsamples from the experimental solutions were extracted and centrifuged, before complexation with ferrozine, and the absorbance was corrected using a blank containing DI water and ferrozine. Chlorate concentrations were measured at the start and the end of the experiment, using a Dionex Integrion high pressure ion chromatograph (Thermo Scientific, Sunnyvale, CA, USA) equipped with an IonPac AS11 analytical column, ADRS 600 suppressor, and conductivity detector with a 12 mmol L^{-1} KOH eluent. The total iron [Fe(II) and Fe(III)] in the solutions after the end of the experiments were measured using an iCAP 7400 Duo inductively coupled plasma optical emission spectroscopy (Thermo Scientific, Madison, WI, USA).

A kinetic rate law model for dissolved Fe(II) oxidation by chlorate [63–65] was previously implemented in The Geochemist's Workbench module React [49], using a modified LLNL database [86,87]. This kinetic model was employed in the present study to simulate the reaction of chlorate with Fe(II), using the starting compositions of the experiments. Details of the kinetic model, rate constants, and the activation energy can be found in our previous paper [49].

2.2. Mineral Precipitation Studies

The Fe(II) oxidation products were studied for a range of fluid compositions and Fe(II):ClO_3^- ratios by conducting experiments at larger volumes (150 mL) to facilitate greater solid phase production needed for characterization (Table 2). The experimental solutions for the higher volume mineral precipitation experiments were prepared in serum bottles and sealed inside the anaerobic chamber and then placed on an orbital shaker outside the chambers, operating at ~160 rotations per minute for ~100 days. A control sample containing dissolved Fe(II) but no chlorate at pH 7 was similarly prepared in a serum-bottle reactor to verify the effectiveness of using sealed serum bottles, outside the anaerobic chamber for anaerobic experiments. The suspensions were then filtered (0.22 μm pore size MCE membrane) and dried inside the anaerobic chamber, using a vacuum desiccator. The solid samples were analyzed by powder X-ray diffraction (XRD) using a D8 Advance diffractometer (Bruker AXS, Karlsruhe, Germany) equipped with a Cu Kα source and a position sensitive, energy-dispersive LynxEye XE detector. Diffrac.Eva version 4.0 (Bruker AXS, Karlsruhe, Germany) was used for mineral identification, and the Profex version 4.2 [88] interface to BGMN [89] was used for quantitative phase analysis via the Rietveld method.

3. Results

3.1. Iron Oxidation in Chlorate-Equivalent vs. Chlorate-Deficient Systems

The experiments in both chlorate-equivalent systems ([Fe(II)]/[ClO_3^-] ≈ 6) and chlorate-deficient systems ([Fe(II)]/[ClO_3^-] > 6) displayed a decrease in their Fe(II) concentration and pH with time (Figure 1, Table 1). The pH dropped to ~2 in chloride- and ~2.5 in sulfate-rich fluids, in response to Fe(II) oxidation and subsequent Fe(III) hydrolysis. Similar to Mitra and Catalano [49], the rate of Fe(II) oxidation was slower in sulfate- than chloride-rich fluids, despite the greater Fe(II) to chlorate ratios in the present study. Fe(II) oxidation in chlorate-equivalent systems for all fluids and initial pH conditions displayed about 90% of the maximum stoichiometric extent of reaction within 100 days. The chlorate-equivalent systems experienced a greater extent of Fe(II) oxidation than chlorate-deficient systems, due to the stoichiometrically greater amount of chlorate in the system.

The rate of Fe(II) oxidation by chlorate was proportional to the chlorate concentration [63], explaining the slower oxidation rate in chlorate-deficient systems than the chlorate-equivalent and "chlorate-excess" systems ([Fe(II)]/[ClO_3^-] ≈ 1) [49]. Unlike chlorate-equivalent systems that contain nearly enough chlorate to oxidize all dissolved Fe(II), the chlorate-deficient systems were expected to contain excess substantial Fe(II) ions after the consumption of all available chlorate in the solutions. The small amount of dissolved Fe(II) unoxidized in the chlorate-equivalent experiments was due to the slightly greater [Fe(II)]/[ClO_3^-] than 6 and the insufficient time to undergo full oxidation. The pH evolution trend matched the Fe(II) reduction trend and the chlorate-deficient systems showed a slower pH decrease than the chlorate-equivalent systems. This effect was expressed more clearly in sulfate- than in chloride-fluids, owing to the slightly slower Fe(II) oxidation rate. At the end of the experiments, the chlorate in all reactors was below the detection limit (0.012 mmol L^{-1}) (Table 1).

To further evaluate the stoichiometric efficiency of chlorate, the kinetic data were compared to the predictions of the rate model from Mitra and Catalano [49], which followed the following rate law [63–65]:

$$-\frac{d[Fe(II)]}{dt} = k_1 a_{Fe^{2+}} a_{ClO_3^-} a_{H^+}^{0.886} + k_2 a_{Fe^{2+}} a_{ClO_3^-} a_{H^+}^{-0.634} \quad (2)$$

This model explicitly assumed a 100% efficiency, i.e., 1 mole of ClO_3^- oxidized 6 moles of Fe(II). In other words, the kinetic model provided the ideal extent and rate of Fe(II) oxidation, chlorate consumption, and pH evolution, as a function of time corresponding to each experiment. The results of the experimental studies were compared to the model results to understand the practical efficiency of chlorate to oxidize Fe(II) in experimental conditions. Both Fe(II) concentration and the pH of the experiments were in close agreement with predictions of our previously-parameterized kinetic model [49], across near-neutral to acidic pH conditions in both chloride- and sulfate-rich fluid systems

(Figure 1). The kinetic model also predicted near-complete consumption of chlorate (Figure S2), as observed in the experiments (Table 1) at the end of ~100 days. This model-data comparison demonstrated that chlorate expressed its maximum capacity for oxidizing dissolved Fe(II) in Mars-relevant fluids.

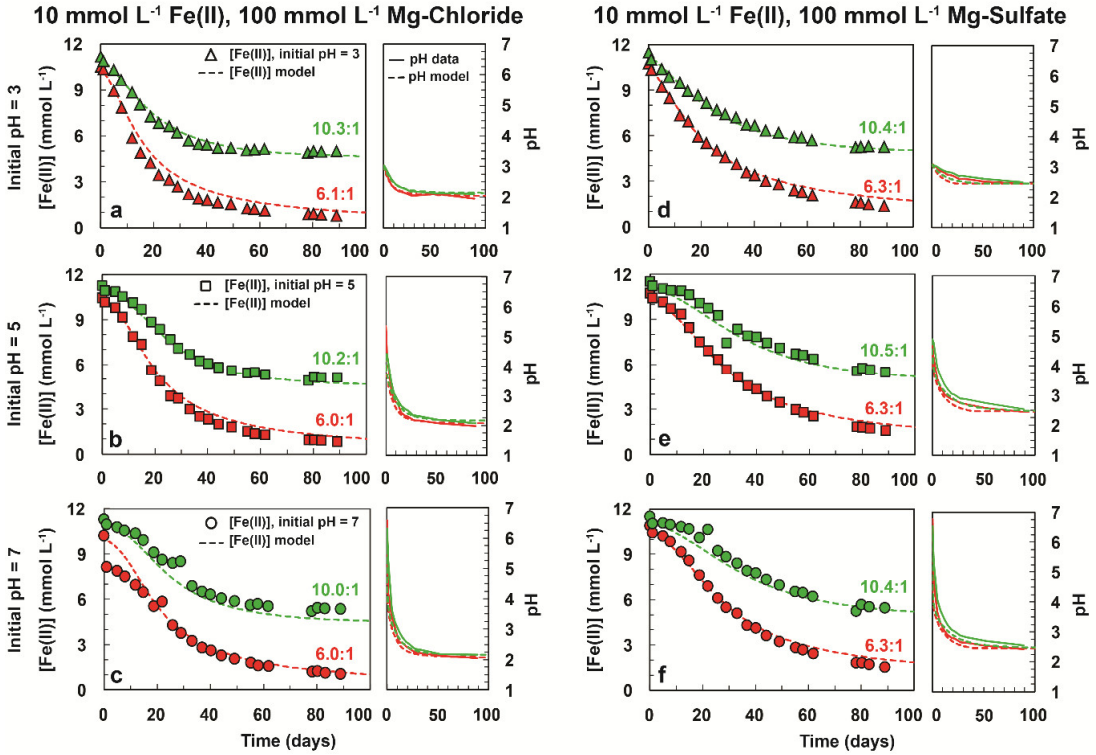

Figure 1. The dissolved Fe(II) concentration and pH versus time in systems containing approximately 10 mmol L^{-1} Fe(II) with 1.67 ([Fe(II)]/[ClO_3^-] ≈ 6) mmol L^{-1} and 1 mmol L^{-1} (≈10) ClO_3^- in 10^{-1} mol L^{-1} $MgCl_2$ at initial (**a**) pH 3, (**b**) pH 5, and (**c**) pH 7, and in 10^{-1} mol L^{-1} $MgSO_4$ fluids at initial (**d**) pH 3, (**e**) pH 5, and (**f**) pH 7 at 24 °C. The ratios written alongside the curves represent the initial molar ratio between [Fe(II)] and [ClO_3^-].

Table 1. Fluid composition of the kinetic experiments.

Sample [a]	Initial $[Fe^{2+}]$ (mmol L^{-1})	Initial $[ClO_3^-]$ (mmol L^{-1})	$[Fe^{2+}]/[ClO_3^-]$	Initial pH	Model Final $[Fe^{2+}]$ (mmol L^{-1}) [b]	Experimental Final $[Fe^{2+}]$ (mmol L^{-1}) [b]	Final $[ClO_3^-]$ (mmol L^{-1})	Model Final pH [d]	Experimental Final pH [d]
Cl-6:1-10-100-3	10.5	1.73	6.1	3.04	0.98	0.65	BDL [c]	2.05	1.96
Cl-6:1-10-100-5	10.4	1.73	6.0	5.34	1.03	0.84	BDL	2.07	1.98
Cl-6:1-10-100-7	10.2	1.70	6.0	6.58	1.01	0.49	BDL	2.08	2.04
Cl-10:1-10-100-3	11.1	1.08	10.3	3.02	4.68	4.99	BDL	2.14	2.01
Cl-10:1-10-100-5	11.2	1.10	10.2	4.34	4.67	5.09	BDL	2.16	2.07
Cl-10:1-10-100-7	11.3	1.13	10.0	6.31	4.57	5.36	BDL	2.16	2.16
S-6:1-10-100-3	10.8	1.71	6.3	3.07	1.70	0.93	BDL	2.45	2.44
S-6:1-10-100-5	10.7	1.71	6.3	4.68	1.81	0.96	BDL	2.45	2.44
S-6:1-10-100-7	10.9	1.73	6.3	6.77	1.82	0.95	BDL	2.45	2.43
S-10:1-10-100-3	11.5	1.10	10.4	3.06	5.02	5.28	BDL	2.45	2.49
S-10:1-10-100-5	11.5	1.10	10.5	4.88	5.19	5.46	BDL	2.48	2.53
S-10:1-10-100-7	11.5	1.10	10.4	6.54	5.18	5.44	BDL	2.48	2.55

[a] Sample name code: The abbreviated names of each experiment represent the fluid composition (either Cl = chloride, or S = sulfate), ratio of iron (II) to chlorate (either ≈6:1 or ≈10:1), concentration of Fe(II) in mmol L^{-1}, concentration of background salt ($MgCl_2$ or $MgSO_4$) in mmol L^{-1} and the initial pH. [b] Concentration ~100 days after the start of the experiments. [c] Below detection limit (0.012 mmol L^{-1}). [d] pH ~100 days after the start of the experiments.

3.2. Mineral Products in Chlorate-Equivalent vs. Chlorate-Deficient Systems

Fe(II) oxidation by chlorate and subsequent Fe(III) hydrolysis yielded diverse mineral products in the corresponding ~100 day duration replicate mineral precipitation experiments (Figure 2, Table 2). The final chlorate concentration in all replicate experiments dropped below the detection limit of the ion chromatograph (Table 2). The final pH values of the replicate solutions matched with the final pH values of the corresponding kinetic experiments (Table 1), except the solutions starting at near-neutral solutions, in which minor deviation in the final pH was observed. The chloride fluids that started at pH 3 primarily produced dissolved Fe(III), and filtering the solution did not yield sufficient minerals for characterization. The final pH of these solutions dropped below pH 2, facilitating greater solubility of the generated Fe(III) and leading to decreased amounts of mineral precipitation. A portion of the minerals that formed in these solutions were likely nanoparticulates and passed through the filter due to their small particle size. Discoloration indicated that particles were also retained by the filter membrane but these remained embedded and could not be recovered for analysis. The remainder of the precipitate was too limited in quantity to recover and analyze. All remaining experiments yielded mineral precipitates that depended on the fluid composition, the extent of Fe(II) oxidation, and the reaction rate (Figure 2).

3.2.1. Minerals Produced in Chloride-Rich Fluids

The chloride-rich fluid solutions that started at pH ~7, unlike pH 3, produced a mixture of Fe(III)- and mixed-valent Fe(II/III) minerals (Figure 2a,b, Tables 2, and Table S1). Chlorate-equivalent experimental solutions that started at pH 7 produced a mixture of lepidocrocite, nanocrystalline goethite, and nonstoichiometric magnetite. The proportion of lepidocrocite in the mineral precipitate was greater for higher concentrations of Fe(II) and chloride in the solution. In contrast, chlorate-deficient systems formed a mixture of green rust, goethite, and magnetite. The low-concentration ([Fe(II)] ≈ 10 mmol L^{-1}) chlorate-deficient system preserved green rust while high-concentration ([Fe(II)] ≈ 100 mmol L^{-1}) solutions yielded a larger proportion of magnetite over goethite and green rust. Magnetite precipitated as the dominant mineral in chlorate-deficient chloride fluid systems starting at near-neutral conditions, in both low ([Fe(II)] ≈ 10 mmol L^{-1}) and high ([Fe(II)] ≈ 100 mmol L^{-1}) concentration solutions. The high-concentration chlorate-deficient system showed formation of magnetite with minor goethite. The chlorate-deficient systems maintained substantial unreacted Fe(II) and produced slower oxidation rates and relatively higher pH values, which facilitated the predominance of magnetite over other Fe(III) minerals.

3.2.2. Minerals Produced in Sulfate-Rich Fluids

All experiments conducted in the sulfate-rich fluid systems yielded mineral precipitates containing either magnetite, goethite, or schwertmannite (Figure 2c,d, Table 2, and Table S1). The SO_4-rich fluids did not precipitate lepidocrocite or green rust. The experimental solutions that started at pH 3 produced either schwertmannite or goethite, depending on the Fe(II) concentration. Solutions with high solute concentration ([Fe(II)] ≈ 100 mmol L^{-1}) formed schwertmannite as the sole phase. The final pH of these solutions dropped below pH ~2.3 and no other Fe(III)-bearing phases co-existed with schwertmannite. The solutions containing low solute concentrations ([Fe(II)] ≈ 10 mmol L^{-1}) starting at initial pH 3, precipitated nanocrystalline goethite instead of schwertmannite. Experimental solutions that started at pH 7 produced magnetite or more crystalline goethite. The proportion of crystalline goethite also increased in solutions that started at near neutral solutions.

Table 2. Fluid composition of the mineral precipitation studies.

Sample [a]	Initial $[Fe^{2+}]$ (mmol L^{-1})	Initial $[ClO_3^-]$ (mmol L^{-1})	Initial $[Fe^{2+}]/[ClO_3^-]$	Initial pH	Model Final $[Fe^{2+}]$ (mmol L^{-1})	Experimental Final $[Fe^{2+}]$ (mmol L^{-1})	Final Total [Fe] (mmol L^{-1})	Final $[ClO_3^-]$ (mmol L^{-1})	Final pH	Mineral Products
Cl-6:1-10-100-3	11.6	1.92	6.1	3.08	0.12	1.53	4.11	BDL [b]	1.95	Trace [c]
Cl-6:1-10-100-7	8.00	1.42	5.6	7.02	0.00	2.14	1.96	BDL	2.51	M,G,L
Cl-6:1-100-100-3	90.1	15.5	5.8	3.00	0.00	0.57	43.6	BDL	1.56	Trace
Cl-6:1-100-100-7	90.9	15.1	6.0	7.25	0.16	0.35	0.35	BDL	2.54	L,M,G
Cl-10:1-10-100-3	12.5	1.35	9.3	3.04	4.43	3.12	6.47	BDL	1.92	Trace
Cl-10:1-10-100-7	13.2	1.32	10.0	7.02	5.28	0.00	0.13	BDL	5.74	M,G,GR
Cl-10:1-100-100-3	138	15.0	9.2	2.97	48.1	39.0	89.4	BDL	1.46	Trace
Cl-10:1-100-100-7	141	15.3	9.2	7.26	49.0	10.9	11.5	BDL	4.46	M,G
S-6:1-5-100-3	3.85	0.63	6.1	3.01	0.07	1.57	2.24	BDL	2.72	Trace
S-6:1-5-100-7	3.91	0.63	6.2	6.90	0.13	0.82	0.10	BDL	4.60	M,G
S-6:1-10-100-3	8.82	1.49	5.9	3.04	0.00	1.47	3.43	BDL	2.51	G
S-6:1-10-100-7	8.61	1.45	6.0	6.80	0.00	1.74	3.48	BDL	2.58	G
S-6:1-100-100-3	83.5	15.2	5.5	3.04	0.00	0.31	50.2	BDL	2.11	S
S-6:1-100-100-7	72.5	15.2	4.8	6.64	0.00	0.23	12.1	BDL	2.08	G
S-10:1-10-100-3	9.53	1.01	9.4	3.01	3.47	3.33	5.71	BDL	2.58	G
S-10:1-10-100-7	9.48	1.01	9.4	7.02	3.42	5.03	4.99	BDL	3.43	M,G
S-10:1-100-100-3	96.4	9.65	10.0	3.03	38.5	18.6	58.9	BDL	2.25	S
S-10:1-100-100-7	97.1	10.2	9.5	7.04	36.0	15.6	28.6	BDL	2.21	G

[a] Sample name code: The abbreviated names of each experiment represent the fluid composition (either Cl = chloride, or S = sulfate), ratio of iron(II) to chlorate (≈6:1 or ≈10:1), Fe(II) concentration in mmol L^{-1}, background salt concentration ($MgCl_2$ or $MgSO_4$) in mmol L^{-1} and the initial pH. [b] Below detection limit (0.012 mmol L^{-1}). [c] The experiment did not generate enough iron oxides for characterization. Mineral codes: G = Goethite, L = Lepidocrocite, M = Magnetite, GR = Green Rust, S= Schwertmannite, and Sa = Salt.

Sulfate-rich solutions containing greater than ~10 mmol L^{-1} Fe(II) precipitated magnetite as the predominant mineral in chlorate-deficient systems at neutral pH. On the other hand, analogous chlorate-equivalent systems did not precipitate magnetite. We investigated a chlorate-equivalent solution with even lower solute concentrations ([Fe(II)] ≈ 5 mmol L^{-1}) to further decrease the rate of Fe(II) oxidation. Magnetite precipitated with minor goethite in this dilute chlorate-equivalent system, when the initial pH was 7 but did not form any detectable mineral precipitate in solution that started at pH 3. The precipitation of magnetite was favored over goethite in this system, owing to the very slow Fe(II) oxidation rate, due to low initial [Fe(II)] and the mild acidic nature of the final fluid (pH_{final} ≈ 4.6).

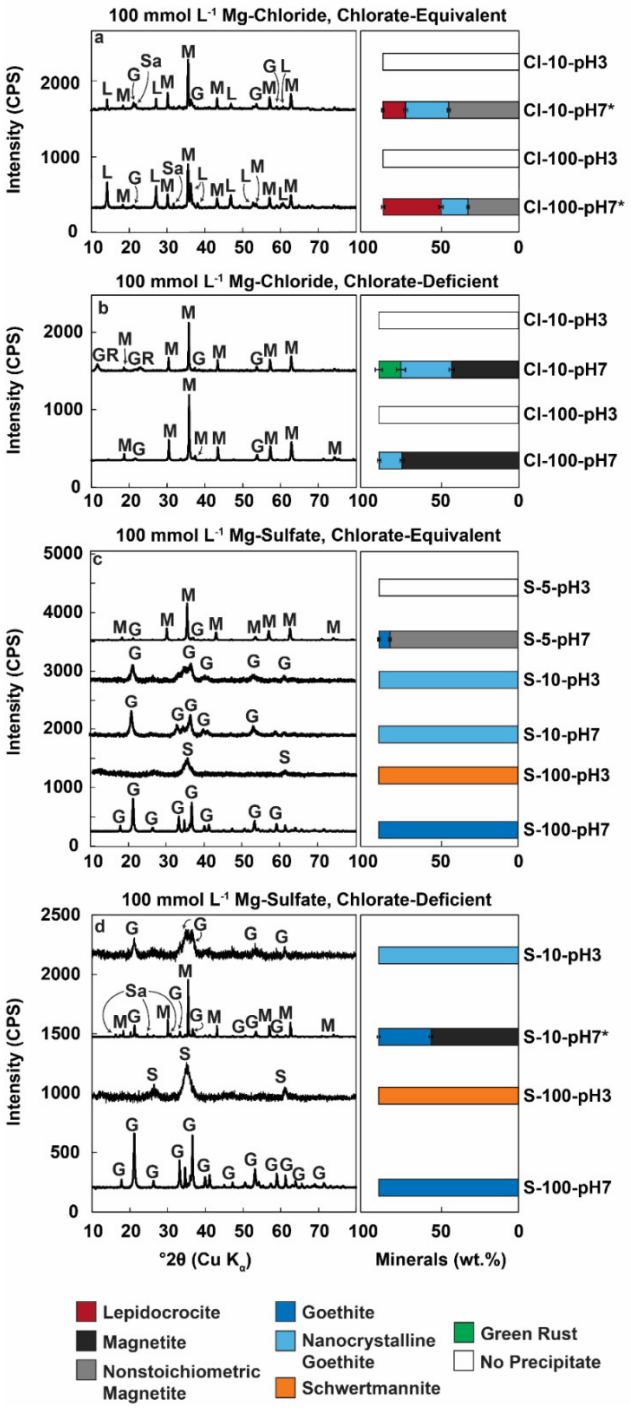

Figure 2. XRD patterns of the mineral products (left) and phase proportions generated using Rietveld refinement (right) for the corresponding XRD scans (Figures S3–S6) of the precipitates formed by the oxidation of dissolved Fe(II) by chlorate (ClO_3^-). Chloride-rich fluids using (**a**) [Fe(II)]/[ClO_3^-] ≈ 6 and

(**b**) [Fe(II)]/[ClO_3^-] ≈ 10 and sulfate-rich fluids using (**c**) [Fe(II)]/[ClO_3^-] ≈ 6 and (**d**) [Fe(II)]/[ClO_3^-] ≈ 10 were investigated. The sample labels depict fluid type, initial Fe(II) concentration (mmol L^{-1}), $MgCl_2$ concentration (mmol L^{-1}), and initial pH (sample label details in Table 2, except segregated by initial Fe(II) to chlorate ratio). The abbreviated names of each experiment represent the fluid composition (either Cl = chloride, or S = sulfate), concentration of Fe(II) in mmol L^{-1}, and the initial pH. Diagnostic peaks are as follows: G = Goethite, L = Lepidocrocite, M = Magnetite, GR = Green Rust, S = Schwertmannite, and Sa = Salt (bischofite [$MgCl_2 \cdot 6H_2O$], halite [NaCl], or hexahydrite [$MgSO_4 \cdot 6H_2O$]). The scans are offset from each other and scaled for better visualization; CPS = counts per second.

4. Discussion

4.1. Fe(II) Oxidation Capacity of Chlorate

Our results demonstrated that chlorate expresses the full theoretical capacity to oxidize Fe(II) in Mars-relevant fluid systems. The final observed dissolved Fe(II) concentration in all experimental solutions at the end of ~100 days were similar to the calculated final values predicted in the same time period by the kinetic model (Tables 1 and 2), which assumed full oxidation efficiency of chlorate ions. The close agreement between the experiment and the model (Figure 1) demonstrated that each chlorate ion could oxidize six dissolved Fe(II) ions without substantial loss via side-reactions. Therefore, any chlorate present on the surface of Mars is expected to be fully available to react with Fe(II), providing a substantial oxidizing capacity. This also confirmed the applicability of the previously published rate law model [49] to accurately predict the rate of Fe(II) oxidation by chlorate in diverse systems. The model can therefore be confidently used to simulate Fe(II) oxidation by chlorate in diverse Mars-relevant fluids.

4.2. Geochemical Parameters Determining Mineral Products

4.2.1. Fluid Composition

The fluid composition, specifically the dominant anion present, exerts strong control over the mineral product by influencing the mineral formation pathways [24] and by providing essential components for some minerals (e.g., chloride for akaganeite, sulfate for schwertmannite and jarosite) (Figure 3). The effect of fluid composition on the nature of mineral product formation is shown in our results (Figure 2) and our earlier study [49]. Iron oxidation by chlorate in chloride-rich fluids produced either lepidocrocite, goethite, magnetite, akaganeite, or a mix of these minerals. Chloride and other halogenides (bromide, iodide, fluoride) promote lepidocrocite formation [90,91], and akaganeite forms in acidic chloride-rich fluids [24,92–95]. Similarly, in sulfate-rich solutions iron oxidation by chlorate produced either goethite, magnetite, schwertmannite, jarosite, or a combination of these minerals. The precipitation of jarosite (hydronium- and natro-) was observed by Mitra and Catalano [49]. Sulfate ions also favors goethite formation over lepidocrocite [24], hence the predominance of goethite in sulfate-rich fluids. Schwertmannite forms as a precursor mineral to jarosite and goethite in Fe(II) oxidizing sulfate-rich fluids [96–98].

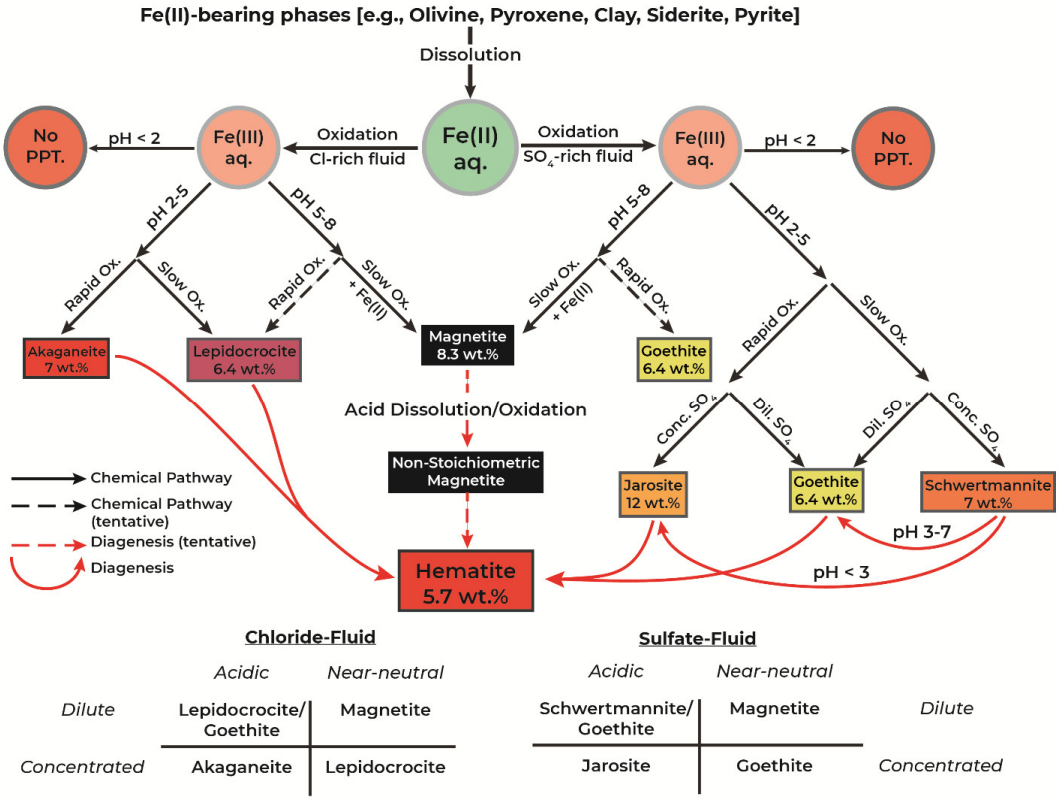

Figure 3. (Top) Schematic of possible iron oxidation pathways on Mars. Mineral products of iron oxidation determined by the fluid type, solution pH, and oxidation rate. The wt.% in each mineral box represents the amount of Fe(III)-bearing mineral that can be produced by the oxidation of Fe(II) by 1 wt.% chlorate. (Below) Fourfold diagram depicting the dominant mineral product as a function of fluid concentration and solution pH.

4.2.2. pH Evolution

The solution pH also played an important role in determining the type and proportion of the mineral precipitate (Figure 3). Highly acidic systems inhibited the precipitation of substantial Fe(III) minerals because of mineral nucleation inhibition and the weak supersaturation of iron oxides at low pH (<2) (Figure 2, Table 2). When minerals do form in substantial quantities, the final pH alone does not determine the parameter of the mineralogy, as the data clearly demonstrated that this was affected by the pH at the time of nucleation. The fluids at the end of the experiments were acidic; this suggest that phases such as akaganeite [$Fe_8O_{6.4}(OH)_{9.7}Cl_{1.3}$ or β-FeO(OH,Cl)] and jarosite [$XFe_3(OH)_6(SO_4)_2$, X = K^+, Na^+ or H_3O^+] should form. However, green rust and magnetite, which typically form in near neutral and alkaline conditions [24], formed in some cases, with goethite and lepidocrocite also occurring. This indicated that the circumneutral pH at the time of mineral nucleation had a substantial effect on the fate of Fe(III).

The relative abundance of goethite and schwertmannite in sulfate-rich systems was also primarily controlled by the solution pH. Schwertmannite is a common mineral in acid sulfate systems and was shown to occur between pH 4.7 to 1.9 [98]. It is a metastable precursor mineral forming in oxidizing sulfate-rich Fe(II) solutions in acidic systems [96,97]. The stability of schwertmannite in our experiments might thus be transient, although it is apparently stable in the studied fluids for at least 100 days. In other studies schwertmannite was shown to transform to either goethite or jarosite, depending on the pH and sulfate concentration of the solution [97,99–104]. In the present work, schwertmannite formed only in experimental solutions that started at pH ~3 and then dropped below pH ~2.3. The preservation of schwertmannite in our experiments demonstrated the important role played by the solution pH at the time of mineral nucleation, in determining the type of mineral precipitate.

The frequent occurrence of magnetite was unexpected, given the low final pH of some experiments. Notably, magnetite only precipitated in solutions that started at near-neutral pH. The solution pH at the time of magnetite nucleation was likely ~4. Simulation of the exact initial composition of the experiment using the kinetic model found that the pH was at this value at the initiation of magnetite precipitation (simulation not shown). Magnetite is metastable in acidic solutions, owing to its high solubility [105,106]. It persists in our experimental solutions either due to slow dissolution kinetics [107,108], or the formation of an oxidized surface layer that inhibited further dissolution. Lattice parameters and octahedral iron occupancies from Rietveld refinements of the XRD results indicate the presence of non-stoichiometric magnetite in a number of experiments (Figure 2). Non-stoichiometric magnetite, also referred to as "cation-deficient magnetite", had an Fe(II)/Fe(III) ratio <0.5 and a unit cell smaller than regular magnetite (8.396 Å), caused by Fe(II) oxidation to Fe(III), and the presence of vacancies in its structure [109]. The formation of non-stoichiometric magnetite might be caused either by direct oxidation of magnetite by chlorate or by the leaching of surficial Fe(II) ions of magnetite in acidic fluids (pH 2–2.5) [110]. Our experiments depicted a similar case in which magnetite at the end of the experiment was retrieved from acidic solutions.

4.2.3. Oxidation Rate

Geochemically similar systems can produce different mineral products due to the differences in their iron oxidation rate (Figure 3). The oxidation rate is primarily controlled by the reactant concentration ([Fe(II)] and [ClO_3^-]) (Equation(2)) [63–65], with dilute solutions experiencing slower oxidation rate than solutions with higher concentrations. Chloride-rich, "Chlorate-excess" ([Fe(II)]/[ClO_3^-] ≈ 1) solutions investigated in our prior investigation [49] produced akaganeite, due to very rapid oxidation rates. In contrast, lepidocrocite formed in similar fluids in the chlorate-equivalent systems of the present study due to slower rate of Fe(II) oxidation (Figure 2).

Slower rates of oxidation in chloride-rich, chlorate-deficient systems induced magnetite formation over lepidocrocite for initially circumneutral pH conditions. On the contrary, during faster Fe(II) oxidation, lepidocrocite formation is preferred over magnetite (Figure S7). The figure demonstrates how the mineral type is a strong function of the oxidation rate. A mixture of lepidocrocite and goethite is formed in near-neutral solutions if the rate of formation is slightly slower [111]. In chloride-rich fluids, systems favoring faster iron oxidation form akaganeite [49], while those yielding slower oxidation rates form lepidocrocite and magnetite.

Similar to the chloride system, for sulfate-rich fluids the chlorate-excess solutions studied previously produced jarosite in higher concentration solutions ([Fe(II)] ≈ [ClO_3^-] ≈ 100 mmol L^{-1}) that yielded relatively fast oxidation, while lower concentration solutions ([Fe(II)] ≈ [ClO_3^-] ≈ 10 mmol L^{-1}) favored goethite [49]. Slower oxidation rates in chlorate-equivalent and -deficient systems produced either goethite, schwertmannite, or magnetite. Relatively faster oxidation rates favored goethite (or schwertmannite, depending on initial pH) production over magnetite. The sulfate-rich fluids produced magnetite in systems with an even slower oxidation rate, which contained unoxidized Fe(II) along with oxidized Fe(III) in the solution. Magnetite formed either in chlorate-deficient systems containing low [Fe(II)] (~10 mmol L^{-1}) (e.g., S-10:1-10-100-7) or in chlorate-equivalent systems with even lower [Fe(II)] (~5 mmol L^{-1}) (e.g., S-6:1-5-100-7); refer to Tables 1 and 2 footnotes for explanation of the sample codes. In all systems, magnetite formed in solutions undergoing slow oxidation at near-neutral solutions (Figure S7). Sulfate-rich solutions produced magnetite only when the rate of oxidation was orders of magnitude slower than those which formed goethite or jarosite.

4.3. Quantitative Measure of Mineral Production

The Fe(III) ions produced by Fe(II) oxidation undergo hydrolysis and precipitate Fe(III)-bearing and mixed valence Fe(II/III) minerals. Mass balance calculations showed that 1 wt.% chlorate could produce about 6.4 wt.% FeOOH (e.g., goethite, lepidocrocite). Similarly, if other chemical species, such as chloride and sulfate, were available, 1 wt.% chlorate could produce ~12 wt.% jarosite [$XFe_3(OH)_6(SO_4)_2$, X = K^+, Na^+ or H_3O^+], ~7 wt.% schwertmannite [($\sim Fe_8O_8(OH)_6SO_4$], and ~7 wt.%

akaganeite [$Fe_8O_{6.4}(OH)_{9.7}Cl_{1.3}$]. In systems with slow oxidation rates, the Fe(III) generated from 1 wt.% chlorate might combine with unreacted Fe(II) to form ~8.3 wt.% magnetite. Diagenetic transformation of these metastable phases [24,25,33–44] yield about 5.7 wt.% hematite per wt.% of chlorate reacted.

Such diagenetic transformations are critical to the ultimate fate of iron oxides and oxyhydroxides that occur as metastable phases on the Martian surface [112]. Although ferrihydrite was not one of the phases observed to form in our study, the timescales of its phase transformation provides insight into hematite formation via diagenesis on Mars. Ferrihydrite transforms in aqueous media to hematite, on timescales of years to decades, at temperatures as low as 4 °C, with the rate being primarily dependent on pH, temperature, and the presence of solutes or other minerals in the solution [113–119]. The extent of any diagenetic transformation is primarily a function of time and temperature [120], and mineral transformation processes studied at high temperature in the laboratory might occur during diagenesis at lower temperature after increased reaction times, unless other pathways take over. Goethite decomposes directly to hematite, through thermal or hydrothermal dehydroxylation processes [24] and by dehydration [33]. Goethite can also transform to hematite at ~25 °C, during diagenesis in geological conditions, in the presence of liquid water [26]. Goethite is the most common Fe(III) bearing mineral that formed in our study (Figure 2) and likely produces hematite, given the right conditions or time. Based on morphological [34] and spectral studies [27], goethite formed in an aqueous environment was considered to be the most probable precursor mineral for crystalline hematite spherules at Meridiani Planum [25,27,33]. Lepidocrocite, albeit a goethite polymorph, does not form hematite directly but involves maghemite (γ-Fe_2O_3) as an intermediate. In our work, lepidocrocite formed in chloride-rich (Figure 2) and perchlorate-rich solutions [49].

Akaganeite, schwertmannite, and jarosite can undergo transformation to hematite in both aqueous solution and through solid-state transformation. Akaganeite transforms to hematite via a dissolution-reprecipitation mechanism at ambient (~28 °C) [35] and hydrothermal (70–200 °C) [36,37,121–124] conditions. The solution pH and the presence of other solutes are important parameters that govern akaganeite transformation [121], with goethite forming instead of hematite at pH > 12. Akaganeite transformation to hematite in hydrothermal systems sometimes precedes with the early formation of hydrohematite, an Fe-deficient, hydroxyl (-OH)rich hematite phase [124]. Akaganeite can also transform to jarosite at lower pH conditions (<pH 4.5) in the presence of sulfate [92]. Akaganeite precipitated in chloride-rich, chlorate-excess solutions [49], and could serve as important hematite precursors on Mars. An iron oxidation study [96] conducted on sulfate-rich systems demonstrated the transformation of jarosite and nanocrystalline goethite to hematite, which might explain the association of hematite and sulfates in regions like Valles Marineris [125,126], Aureum Chaos, and Iani Chaos [127]. Schwertmannite transforms to goethite at high pH, while jarosite is favored at low pH conditions [96,97,99–104]. Although schwertmannite could be stable in the solid-state for longer periods of time (e.g., Rio Tinto) [128], it often readily transforms to either jarosite or goethite [96,97,99–104], depending on the solution pH and sulfate concentration. Schwertmannite and jarosite are important Fe(III)-bearing minerals in sulfate-bearing fluids in our experiments. While jarosite precipitated only in the chlorate-excess systems [49], schwertmannite formed in both chlorate-equivalent and -deficient systems. The ability of schwertmannite to form goethite or jarosite provides additional potential diagenetic routes to hematite on Mars.

4.4. Implications for Gale Crater, Mars

Chlorate is likely present in Gale Crater, as suggested by in-situ SAM instrument results [51,53,54,129] and recent terrestrial laboratory experiments [55]. Chlorate is now shown to form all key iron oxides found in Gale Crater via Fe(II) oxidation (Figure 2 and [49]), except hematite, and was recently proposed to be a likely Fe(II) oxidant [130]. However, hematite is expected as a diagenetic product of many of these phases (Section 4.3). The results from the CheMin drill samples in Gale crater on Mars show coexistence of magnetite and akaganeite in the Yellowknife Bay Formation [John Klein (JK), and Cumberland (CB) drill samples] [131], and magnetite with jarosite in the Murray

Formation [Confidence Hills (CH), Mojave2 (MJ), Telegraph Peak (TP), and Stoer (ST) drill samples] [6,7]. Based on the results of our studies, none of the experiments generated coexisting akaganeite and magnetite, or jarosite and magnetite. It is therefore likely that magnetite was precipitated from a fluid that was different in composition from those precipitating jarosite and akaganeite (Figure 3). Therefore, the occurrence of hematite as well as magnetite with acidic phases indicates that multiple diagenetic fluids of different compositions have likely altered both Yellowknife Bay and Murray Formation sediments in the past. Alternatively, evaporation processes might concentrate and acidify fluids, and the same near-neutral and dilute fluid that forms magnetite might subsequently evolve into the akaganeite or jarosite stability fields, provided that enough chlorate is present to continue oxidizing residual Fe(II) and that the resulting fluids do not destroy the initial magnetite precipitates.

5. Conclusions

The experimental efficiency of Fe(II) oxidation by chlorate was investigated in Mars-relevant fluids. Chlorate can exhibit its maximum theoretical oxidation capacity in chloride- and sulfate-fluid environments from circumneutral to acidic pH conditions, and closely follows our predictive kinetic model [49]. The mineral products are controlled by the fluid type, acidity, and the Fe(II) oxidation rate. The oxidation rate was determined by the concentration of Fe(II), oxidant (chlorate), and the [Fe(II)]/[chlorate] ratio. Geochemically similar solutions experiencing slower rates of oxidation favored magnetite over other iron oxides. A total of 1 wt.% chlorate can produce ~6.4 wt.% goethite (α-FeOOH) and lepidocrocite (γ-FeOOH), ~7 wt.% akaganeite [β-FeO(OH,Cl)] and schwertmannite [(~$Fe_8O_8(OH)_6SO_4$], ~8.3 wt.% magnetite (Fe_3O_4), and ~12 wt.% jarosite [$XFe_3(OH)_6(SO_4)_2$, X = K^+, Na^+ or H_3O^+]. These phases might subsequently diagenetically convert to ~5.7 wt.% hematite (α-Fe_2O_3). Notably, all iron oxides found in the Gale Crater can be produced by Fe(II) oxidation by chlorate or through subsequent diagenesis. Despite the low concentration on the surface of Mars (<1 wt.%), the high oxidizing capacity of chlorate and its possible regeneration by the putative oxychlorine cycle makes chlorate an important contributor of iron oxide, on both past and present Mars.

Supplementary Materials: The following are available online at www.mdpi.com/2075-163X/10/9/729/s1. Table S1: Mineral proportions and coherent scattering domain sizes determined from Rietveld refinements, Figure S1: [Fe(II)] and pH vs. time for control set-ups of kinetic experiments, Figure S2: Model simulations of chlorate vs. time for kinetic experiments, Figure S3: Rietveld refinement plots for minerals precipitated in Mg-chloride chlorate-equivalent experiments, Figure S4: Rietveld refinement plots for minerals precipitated in Mg-chloride chlorate-deficient experiments, Figure S5: Rietveld refinement plots for minerals precipitated in Mg-sulfate chlorate-equivalent experiments, Figure S6: Rietveld refinement plots for minerals precipitated in Mg-sulfate chlorate-deficient experiments, Figure S7: Model simulations to compare Fe(II) oxidation rate of mineral precipitation studies in relation to the minerals precipitated. The data associated with the manuscript is available at doi:10.6084/m9.figshare.12672308.

Author Contributions: Conceptualization, K.M. and J.G.C.; methodology, K.M. and E.L.M.; software, K.M., J.G.C., and E.L.M.; validation, K.M.; formal analysis, K.M., J.G.C., and E.L.M.; investigation, K.M. and E.L.M.; resources, J.G.C.; data curation, K.M.; writing—original draft preparation, K.M.; writing—review and editing, K.M., J.G.C., and E.L.M.; visualization, K.M. and E.L.M.; supervision, J.G.C.; project administration, J.G.C.; funding acquisition, K.M. and J.G.C. All authors have read and agreed to the published version of the manuscript.

Funding: This research was funded by NASA Science Mission Directorate Future Investigators in NASA Earth and Space Science and Technology (FINESST) program through award no. NNH19ZDA005K.

Acknowledgments: Discussions with Raymond Arvidson and Bradley Jolliff improved this manuscript. Paul Carpenter is thanked for assistance with XRD data collection and Rietveld refinements. Two anonymous reviewers are thanked for insightful comments.

Conflicts of Interest: The authors declare no conflict of interest.

References

1. Christensen, P.R.; Bandfield, J.L.; Clark, R.N.; Edgett, K.S.; Hamilton, V.E.; Hoefen, T.; Kieffer, H.H.; Kuzmin, R.O.; Lane, M.D.; Malin, M.C.; et al. Detection of crystalline hematite mineralization on Mars by the Thermal Emission Spectrometer: Evidence for near-surface water. *J. Geophys. Res. Planets* **2000**, *105*, 9623–9642, doi:10.1029/1999je001093.
2. Lane, M.D.; Morris, R.V.; Mertzman, S.A.; Christensen, P.R. Evidence for platy hematite grains in Sinus Meridiani, Mars. *J. Geophys. Res. Planets* **2002**, *107*, 5126, doi:10.1029/2001je001832.
3. Christensen, P.R.; Wyatt, M.B.; Glotch, T.D.; Rogers, A.D.; Anwar, S.; Arvidson, R.E.; Bandfield, J.L.; Blaney, D.L.; Budney, C.; Calvin, W.M.; et al. Mineralogy at Meridiani Planum from the Mini-TES experiment on the Opportunity Rover. *Science* **2004**, *306*, 1733–1739, doi:10.1126/science.1104909.
4. Klingelhöfer, G.; Morris, R.V.; Bernhardt, B.; Schroder, C.; Rodionov, D.S.; de Souza, P.A.; Yen, A.; Gellert, R.; Evlanov, E.N.; Zubkov, B.; et al. Jarosite and hematite at Meridiani Planum from Opportunity's Mossbauer spectrometer. *Science* **2004**, *306*, 1740–1745, doi:10.1126/science.1104653.
5. Morris, R.V.; Klingelhöfer, G.; Schroder, C.; Rodionov, D.S.; Yen, A.; Ming, D.W.; de Souza, P.A.; Fleischer, I.; Wdowiak, T.; Gellert, R.; et al. Mössbauer mineralogy of rock, soil, and dust at Gusev crater, Mars: Spirit's journey through weakly altered olivine basalt on the plains and pervasively altered basalt in the Columbia Hills. *J. Geophys. Res. Planets* **2006**, *111*, E02S13, doi:10.1029/2005je002584.
6. Rampe, E.; Blake, D.; Bristow, T.; Ming, D.; Vaniman, D.; Morris, R.; Achilles, C.; Chipera, S.; Morrison, S.; Tu, V. Mineralogy and geochemistry of sedimentary rocks and eolian sediments in Gale crater, Mars: A review after six Earth years of exploration with Curiosity. *Geochemistry* **2020**, *80*, 125605, doi:10.1016/j.chemer.2020.125605.
7. Rampe, E.; Ming, D.; Blake, D.; Bristow, T.; Chipera, S.; Grotzinger, J.; Morris, R.; Morrison, S.; Vaniman, D.; Yen, A. Mineralogy of an ancient lacustrine mudstone succession from the Murray formation, Gale crater, Mars. *Earth Planet. Sci. Lett.* **2017**, *471*, 172–185, doi:10.1016/j.epsl.2017.04.021.
8. Bridges, J.C.; Catling, D.; Saxton, J.; Swindle, T.; Lyon, I.; Grady, M. Alteration assemblages in Martian meteorites: Implications for near-surface processes. *Space Sci. Rev.* **2001**, *96*, 365–392, doi:10.1023/A:1011965826553.
9. Vaniman, D.T.; Bish, D.L.; Ming, D.W.; Bristow, T.F.; Morris, R.V.; Blake, D.F.; Chipera, S.J.; Morrison, S.M.; Treiman, A.H.; Rampe, E.B.; et al. Mineralogy of a mudstone at Yellowknife Bay, Gale Crater, Mars. *Science* **2014**, *343*, 1243480, doi:10.1126/science.1243480.
10. Carter, J.; Viviano-Beck, C.; Loizeau, D.; Bishop, J.; Le Deit, L. Orbital detection and implications of akaganeite on Mars. *Icarus* **2015**, *253*, 296–310, doi:10.1016/j.icarus.2015.01.020.
11. Morris, R.V.; Golden, D.C.; Bell, J.F.; Shelfer, T.D.; Scheinost, A.C.; Hinman, N.W.; Furniss, G.; Mertzman, S.A.; Bishop, J.L.; Ming, D.W.; et al. Mineralogy, composition, and alteration of Mars Pathfinder rocks and soils: Evidence from multispectral, elemental, and magnetic data on terrestrial analogue, SNC meteorite, and Pathfinder samples. *J. Geophys. Res. Planets* **2000**, *105*, 1757–1817, doi:10.1029/1999je001059.
12. Milliken, R.E.; Swayze, G.A.; Arvidson, R.E.; Bishop, J.L.; Clark, R.N.; Ehlmann, B.L.; Green, R.O.; Grotzinger, J.P.; Morris, R.V.; Murchie, S.L.; et al. Opaline silica in young deposits on Mars. *Geology* **2008**, *36*, 847–850, doi:10.1130/g24967a.1.
13. Farrand, W.H.; Glotch, T.D.; Rice, J.W.; Hurowitz, J.A.; Swayze, G.A. Discovery of jarosite within the Mawrth Vallis region of Mars: Implications for the geologic history of the region. *Icarus* **2009**, *204*, 478–488, doi:10.1016/j.icarus.2009.07.014.
14. Thollot, P.; Mangold, N.; Ansan, V.; Le Mouelic, S.; Milliken, R.E.; Bishop, J.L.; Weitz, C.M.; Roach, L.H.; Mustard, J.F.; Murchie, S.L. Most Mars minerals in a nutshell: Various alteration phases formed in a single environment in Noctis Labyrinthus. *J. Geophys. Res. Planets* **2012**, *117*, E00J06, doi:10.1029/2011je004028.
15. Weitz, C.M.; Bishop, J.L.; Thollot, P.; Mangold, N.; Roach, L.H. Diverse mineralogies in two troughs of Noctis Labyrinthus, Mars. *Geology* **2011**, *39*, 899–902, doi:10.1130/g32045.1.
16. Ehlmann, B.L.; Mustard, J.F. An in-situ record of major environmental transitions on early Mars at Northeast Syrtis Major. *Geophys. Res. Lett.* **2012**, *39*, 1–7, doi:10.1029/2012gl051594.
17. Liu, Y.; Arvidson, R.E.; Wolff, M.J.; Mellon, M.T.; Catalano, J.G.; Wang, A.; Bishop, J.L. Lambert Albedo retrieval and analyses over Aram Chaos from OMEGA hyperspectral imaging data. *J. Geophys. Res. Planets* **2012**, *117*, doi:10.1029/2012JE004056.

18. Morris, R.V.; Klingelhoefer, G.; Schröder, C.; Rodionov, D.S.; Yen, A.; Ming, D.W.; De Souza, P.; Wdowiak, T.; Fleischer, I.; Gellert, R. Mössbauer mineralogy of rock, soil, and dust at Meridiani Planum, Mars: Opportunity's journey across sulfate-rich outcrop, basaltic sand and dust, and hematite lag deposits. *J. Geophys. Res. Planets* **2006**, *111*, doi:10.1029/2006JE002791.
19. Bradley, J.P.; Harvey, R.P.; McSween, H.Y., Jr. Magnetite whiskers and platelets in the ALH84001 Martian meteorite: Evidence of vapor phase growth. *Geochim. Cosmochim. Acta* **1996**, *60*, 5149–5155, doi:10.1016/S0016-7037(96)00383-3.
20. Morris, R.V.; Klingelhoefer, G.; Bernhardt, B.; Schröder, C.; Rodionov, D.S.; De Souza, P.; Yen, A.; Gellert, R.; Evlanov, E.; Foh, J. Mineralogy at Gusev Crater from the Mössbauer spectrometer on the Spirit Rover. *Science* **2004**, *305*, 833–836, doi:10.1126/science.1100020.
21. Treiman, A.H.; Barrett, R.A.; Gooding, J.L. Preterrestrial aqueous alteration of the Lafayette (SNC) meteorite. *Meteoritics* **1993**, *28*, 86–97, doi:10.1111/j.1945-5100.1993.tb00251.x.
22. Gooding, J.L. Chemical weathering on Mars-thermodynamic stabilities of primary minerals (and their alteration products) from mafic igneous rocks. *Icarus* **1978**, *33*, 483–513, doi:10.1016/0019-1035(78)90186-0.
23. Riveros, P.; Dutrizac, J. The precipitation of hematite from ferric chloride media. *Hydrometallurgy* **1997**, *46*, 85–104, doi:10.1016/S0304-386X(97)00003-0.
24. Cornell, R.M.; Schwertmann, U. *The Iron Oxides: Structure, Properties, Reactions, Occurrences and Uses*, 2nd ed.; John Wiley & Sons: Weinheim, Germany, 2003.
25. Glotch, T.D.; Kraft, M. Thermal transformations of akaganeite and lepidocrocite to hematite: Assessment of possible precursors to Martian crystalline hematite. *Phys. Chem. Miner.* **2008**, *35*, 569–581, doi:10.1007/s00269-008-0249-z.
26. Goss, C.J. The kinetics and reaction-mechanism of the goethite to hematite transformation. *Mineral. Mag.* **1987**, *51*, 437–451, doi:10.1180/minmag.1987.051.361.11.
27. Glotch, T.D.; Morris, R.V.; Christensen, P.R.; Sharp, T.G. Effect of precursor mineralogy on the thermal infrared emission spectra of hematite: Application to Martian hematite mineralization. *J. Geophys. Res. Planets* **2004**, *109*, E07003, doi:10.1029/2003je002224.
28. Gehring, A.; Hofmeister, A. The transformation of lepidocrocite during heating: A magnetic and spectroscopic study. *Clays Clay Miner.* **1994**, *42*, 409–415, doi:10.1346/CCMN.1994.0420405.
29. Gómez-Villacieros, R.; Hernán, L.; Morales, J.; Tirado, J. Textural evolution of synthetic γ-FeOOH during thermal treatment by differential scanning calorimetry. *J. Colloid Interface Sci.* **1984**, *101*, 392–400, doi:10.1016/0021-9797(84)90050-X.
30. Naono, H.; Fujiwara, R.; Sugioka, H.; Sumiya, K.; Yanazawa, H. Micropore formation due to thermal decomposition of acicular microcrystals of β-FeOOH. *J. Colloid Interface Sci.* **1982**, *87*, 317–332, doi:10.1016/0021-9797(82)90329-0.
31. Bigham, J.; Nordstrom, D.K. Iron and aluminum hydroxysulfates from acid sulfate waters. *Rev. Mineral. Geochem.* **2000**, *40*, 351–403, doi:10.2138/rmg.2000.40.7.
32. Stanjek, H.; Weidler, P. The effect of dry heating on the chemistry, surface area, and oxalate solubility of synthetic 2-line and 6-line ferrihydrites. *Clay Miner.* **1992**, *27*, 397–411, doi:10.1180/claymin.1992.027.4.01.
33. Zolotov, M.Y.; Shock, E.L. Formation of jarosite-bearing deposits through aqueous oxidation of pyrite at Meridiani Planum, Mars. *Geophys. Res. Lett.* **2005**, *32*, L21203, doi:10.1029/2005gl024253.
34. Christensen, P.R.; Ruff, S.W.; Fergason, R.L.; Knudson, A.T.; Anwar, S.; Arvidson, R.E.; Bandfield, J.L.; Blaney, D.L.; Budney, C.; Calvin, W.M.; et al. Initial results from the Mini-TES experiment in Gusev crater from the Spirit rover. *Science* **2004**, *305*, 837–842, doi:10.1126/science.1100564.
35. Atkinson, R.; Posner, A.; Quirk, J. Crystal nucleation and growth in hydrolysing iron (III) chloride solutions. *Clays Clay Miner.* **1977**, *25*, 49–56, doi:10.1346/CCMN.1977.0250108.
36. Hamada, S.; Matijevic, E. Ferric hydrous oxide sols IV. Preparation of uniform cubic hematite particles by hydrolysis of ferric-chloride in alcohol-water solutions. *J. Colloid Interface Sci.* **1981**, *84*, 274–277, doi:10.1016/0021-9797(81)90287-3.
37. Hamada, S.; Matijevic, E. Formation of monodispersed colloidal cubic hematite particles in ethanol + water solutions. *J. Chem. Soc. Faraday Trans.* **1982**, *78*, 2147–2156, doi:10.1039/f19827802147.
38. Golden, D.C.; Ming, D.W.; Morris, R.V.; Graff, T.G. Hydrothermal synthesis of hematite spherules and jarosite: Implications for diagenesis and hematite spherule formation in sulfate outcrops at Meridiani Planum, Mars. *Am. Miner.* **2008**, *93*, 1201–1214, doi:10.2138/am.2008.2737.

39. Beitler, B.; Parry, W.T.; Chan, M.A. Fingerprints of fluid flow: Chemical diagenetic history of the Jurassic Navajo sandstone, Southern Utah, U.S.A. *J. Sediment. Res.* **2005**, *75*, 547–561, doi:10.2110/jsr.2005.045.
40. Chan, M.A.; Bowen, B.B.; Parry, W.; Ormö, J. Red rock and red planet diagenesis. *GSA Today* **2005**, *15*, 4–10, doi:10:1130/1052-5173(2005)015.
41. Chan, M.A.; Parry, W.; Bowman, J. Diagenetic hematite and manganese oxides and fault-related fluid flow in Jurassic sandstones, southeastern Utah. *AAPG Bull.* **2000**, *84*, 1281–1310, doi:10.1306/A9673E82-1738-11D7-8645000102C1865D.
42. Reiners, P.W.; Chan, M.A.; Evenson, N.S. (U-Th)/He geochronology and chemical compositions of diagenetic cement, concretions, and fracture-filling oxide minerals in Mesozoic sandstones of the Colorado Plateau. *Geol. Soc. Am. Bull.* **2014**, *126*, 1363–1383, doi:10.1130/b30983.1.
43. Ormö, J.; Komatsu, G.; Chan, M.A.; Beitler, B.; Parry, W.T. Geological features indicative of processes related to the hematite formation in Meridiani Planum and Aram Chaos, Mars: A comparison with diagenetic hematite deposits in southern Utah, USA. *Icarus* **2004**, *171*, 295–316, doi:10.1016/j.icarus.2004.06.001.
44. Potter, S.L.; Chan, M.A.; Petersen, E.U.; Dyar, M.D.; Sklute, E. Characterization of Navajo Sandstone concretions: Mars comparison and criteria for distinguishing diagenetic origins. *Earth Planet. Sci. Lett.* **2011**, *301*, 444–456, doi:10.1016/j.epsl.2010.11.027.
45. Singer, P.C.; Stumm, W. Acidic mine drainage: The rate-determining step. *Science* **1970**, *167*, 1121–1123, doi:10.1126/science.167.3921.1121.
46. Hurowitz, J.A.; Fischer, W.; Tosca, N.J.; Milliken, R.E. Origin of acidic surface waters and the evolution of atmospheric chemistry on early Mars. *Nat. Geosci.* **2010**, *3*, 323–326, doi:10.1038/ngeo831.
47. Nie, N.X.; Dauphas, N.; Greenwood, R.C. Iron and oxygen isotope fractionation during iron UV photo-oxidation: Implications for early Earth and Mars. *Earth Planet. Sci. Lett.* **2017**, *458*, 179–191, doi:10.1016/j.epsl.2016.10.035.
48. Lasne, J.; Noblet, A.; Szopa, C.; Navarro-Gonzalez, R.; Cabane, M.; Poch, O.; Stalport, F.; Francois, P.; Atreya, S.K.; Coll, P. Oxidants at the surface of Mars: A review in light of recent exploration results. *Astrobiology* **2016**, *16*, 977–996, doi:10.1089/ast.2016.1502.
49. Mitra, K.; Catalano, J.G. Chlorate as a potential oxidant on Mars: Rates and products of dissolved Fe(II) oxidation. *J. Geophys. Res. Planets* **2019**, *124*, 2893–2916, doi:10.1029/2019JE006133.
50. Sutter, B.; Quinn, R.C.; Archer, P.D.; Glavin, D.P.; Glotch, T.D.; Kounaves, S.P.; Osterloo, M.M.; Rampe, E.B.; Ming, D.W. Measurements of oxychlorine species on Mars. *Int. J. Astrobiol.* **2017**, *16*, 203–217, doi:10.1017/s1473550416000057.
51. Ming, D.W.; Archer, P.D.; Glavin, D.P.; Eigenbrode, J.L.; Franz, H.B.; Sutter, B.; Brunner, A.E.; Stern, J.C.; Freissinet, C.; McAdam, A.C.; et al. Volatile and organic compositions of sedimentary rocks in Yellowknife Bay, Gale Crater, Mars. *Science* **2014**, *343*, 9, doi:10.1126/science.1245267.
52. Leshin, L.A.; Mahaffy, P.R.; Webster, C.R.; Cabane, M.; Coll, P.; Conrad, P.G.; Archer, P.D.; Atreya, S.K.; Brunner, A.E.; Buch, A.; et al. Volatile, isotope, and organic analysis of Martian fines with the Mars Curiosity Rover. *Science* **2013**, *341*, 1238937, doi:10.1126/science.1238937.
53. Glavin, D.P.; Freissinet, C.; Miller, K.E.; Eigenbrode, J.L.; Brunner, A.E.; Buch, A.; Sutter, B.; Archer, P.D.; Atreya, S.K.; Brinckerhoff, W.B.; et al. Evidence for perchlorates and the origin of chlorinated hydrocarbons detected by SAM at the Rocknest aeolian deposit in Gale Crater. *J. Geophys. Res. Planets* **2013**, *118*, 1955–1973, doi:10.1002/jgre.20144.
54. Sutter, B.; McAdam, A.C.; Mahaffy, P.R.; Ming, D.W.; Edgett, K.S.; Rampe, E.B.; Eigenbrode, J.L.; Franz, H.B.; Freissinet, C.; Grotzinger, J.P.; et al. Evolved gas analyses of sedimentary rocks and eolian sediment in Gale Crater, Mars: Results of the curiosity rover's sample analysis at Mars instrument from Yellowknife Bay to the Namib Dune. *J. Geophys. Res. Planets* **2017**, *122*, 2574–2609, doi:10.1002/2016je005225.
55. Hogancamp, J.; Sutter, B.; Morris, R.; Archer, P.D.; Ming, D.; Rampe, E.; Mahaffy, P.; Navarro-Gonzalez, R. Chlorate/Fe-bearing phase mixtures as a possible source of oxygen and chlorine detected by the Sample Analysis at Mars instrument in Gale Crater, Mars. *J. Geophys. Res. Planets* **2018**, *123*, 2920–2938, doi:10.1029/2018JE005691.
56. Hecht, M.H.; Kounaves, S.P.; Quinn, R.C.; West, S.J.; Young, S.M.M.; Ming, D.W.; Catling, D.C.; Clark, B.C.; Boynton, W.V.; Hoffman, J.; et al. Detection of perchlorate and the soluble chemistry of Martian soil at the Phoenix Lander site. *Science* **2009**, *325*, 64–67, doi:10.1126/science.1172466.

57. Hanley, J.; Chevrier, V.F.; Berget, D.J.; Adams, R.D. Chlorate salts and solutions on Mars. *Geophys. Res. Lett.* **2012**, *39*, L08201, doi:10.1029/2012gl051239.
58. Kounaves, S.P.; Carrier, B.L.; O'Neil, G.D.; Stroble, S.T.; Claire, M.W. Evidence of martian perchlorate, chlorate, and nitrate in Mars meteorite EETA79001: Implications for oxidants and organics. *Icarus* **2014**, *229*, 206–213, doi:10.1016/j.icarus.2013.11.012.
59. Rao, B.; Anderson, T.A.; Redder, A.; Jackson, W.A. Perchlorate formation by ozone oxidation of aqueous chlorine/oxy-chlorine Species: Role of Cl_xO_y radicals. *Environ. Sci. Technol.* **2010**, *44*, 2961–2967, doi:10.1021/es903065f.
60. Jackson, W.A.; Bohlke, J.K.; Andraski, B.J.; Fahlquist, L.; Bexfield, L.; Eckardt, F.D.; Gates, J.B.; Davila, A.F.; McKay, C.P.; Rao, B.; et al. Global patterns and environmental controls of perchlorate and nitrate co-occurrence in arid and semi-arid environments. *Geochim. Cosmochim. Acta* **2015**, *164*, 502–522, doi:10.1016/j.gca.2015.05.016.
61. Brown, G.M.; Gu, B. The chemistry of perchlorate in the environment. In *Perchlorate*; Springer: Boston, MA, USA, 2006; pp. 17–47, doi:10.1007/0-387-31113-0_2.
62. Urbansky, E.T. Perchlorate as an environmental contaminant. *Environ. Sci. Pollut. Res.* **2002**, *9*, 187–192, doi:10.1065/espr2002.05.117.
63. Madlo, K. Kinetics of oxidation of bivalent iron by chlorate. *Collect. Czech. Chem. Commun.* **1979**, *44*, 2760–2768, doi:10.1135/cccc19792760.
64. Ang, K.P.; Creak, G.A.; Kwik, W.L. Effect of ionic-strength on kinetics of oxidation of ferrous ion by chlorate ion. *J. Chem. Soc. Dalton Trans.* **1972**, 2560–2562, doi:10.1039/dt9720002560.
65. Mitzner, R.; Fischer, G.; Leupold, P. Kinetics of oxidation of iron(II) by means of chlorate in perchloric-acid solutions. *Z. Phys. Chem.* **1973**, *253*, 81–95.
66. Higginson, W.C.; Simpson, M.E. Formation of free-radicals in reduction of chlorate by iron(II) cation in dilute aqueous acid solution. *J. Chem. Soc. Chem. Commun.* **1974**, 817–818, doi:10.1039/c39740000817.
67. Miki, H.; Nicol, M. The kinetics of the oxidation of iron(II) by chlorate in the leaching of uranium ores. *Hydrometallurgy* **2009**, *100*, 47–49, doi:10.1016/j.hydromet.2009.10.001.
68. Hong, C.C.; Lenzi, F.; Rapson, W.H. Kinetics and mechanism of chloride-chlorate reaction. *Can. J. Chem. Eng.* **1967**, *45*, 349–355, doi:10.1002/cjce.5450450605.
69. Shakhashiri, B.Z.; Gordon, G. Oxidation of tris(1, 10-phenanthroline) iron (II) ion by chlorate and chlorite ions and chlorine dioxide. *J. Am. Chem. Soc.* **1969**, *91*, 1103–1107.
70. Catling, D.C.; Claire, M.W.; Zahnle, K.J.; Quinn, R.C.; Clark, B.C.; Hecht, M.H.; Kounaves, S. Atmospheric origins of perchlorate on Mars and in the Atacama. *J. Geophys. Res. Planets* **2010**, *115*, E00E11, doi:10.1029/2009je003425.
71. Wu, Z.C.; Wang, A.; Farrell, W.M.; Yan, Y.C.; Wang, K.; Houghton, J.; Jackson, A.W. Forming perchlorates on Mars through plasma chemistry during dust events. *Earth Planet. Sci. Lett.* **2018**, *504*, 94–105, doi:10.1016/j.epsl.2018.08.040.
72. Carrier, B.L.; Kounaves, S.P. The origins of perchlorate in the Martian soil. *Geophys. Res. Lett.* **2015**, *42*, 3739–3745, doi:10.1002/2015gl064290.
73. Turner, A.M.; Abplanalp, M.J.; Kaiser, R.I. Mechanistic studies on the radiolytic decomposition of perchlorates on the Martian surface. *Astrophys. J.* **2016**, *820*, 127, doi:10.3847/0004-637x/820/2/127.
74. Wilson, E.H.; Atreya, S.K.; Kaiser, R.I.; Mahaffy, P.R. Perchlorate formation on Mars through surface radiolysis-initiated atmospheric chemistry: A potential mechanism. *J. Geophys. Res. Planets* **2016**, *121*, 1472–1487, doi:10.1002/2016je005078.
75. Schuttlefield, J.D.; Sambur, J.B.; Gelwicks, M.; Eggleston, C.M.; Parkinson, B.A. Photooxidation of chloride by oxide minerals: Implications for perchlorate on Mars. *J. Am. Chem. Soc.* **2011**, *133*, 17521–17523, doi:10.1021/ja2064878.
76. Squyres, S.W.; Grotzinger, J.P.; Arvidson, R.E.; Bell, J.F.; Calvin, W.; Christensen, P.R.; Clark, B.C.; Crisp, J.A.; Farrand, W.H.; Herkenhoff, K.E.; et al. In situ evidence for an ancient aqueous environment at Meridiani Planum, Mars. *Science* **2004**, *306*, 1709–1714, doi:10.1126/science.1104559.
77. Nuding, D.L.; Rivera-Valentin, E.G.; Davis, R.D.; Gough, R.V.; Chevrier, V.F.; Tolbert, M.A. Deliquescence and efflorescence of calcium perchlorate: An investigation of stable aqueous solutions relevant to Mars. *Icarus* **2014**, *243*, 420–428, doi:10.1016/j.icarus.2014.08.036.
78. Vaniman, D.T.; Bish, D.L.; Chipera, S.J.; Fialips, C.I.; Carey, J.W.; Feldman, W.C. Magnesium sulphate salts and the history of water on Mars. *Nature* **2004**, *431*, 663–665, doi:10.1038/nature02973.

79. Léveille, R.J.; Bridges, J.; Wiens, R.C.; Mangold, N.; Cousin, A.; Lanza, N.; Forni, O.; Ollila, A.; Grotzinger, J.; Clegg, S.; et al. Chemistry of fracture-filling raised ridges in Yellowknife Bay, Gale Crater: Window into past aqueous activity and habitability on Mars. *J. Geophys. Res. Planets* **2014**, *119*, 2398–2415, doi:10.1002/2014je004620.
80. Fox-Powell, M.G.; Hallsworth, J.E.; Cousins, C.R.; Cockell, C.S. Ionic strength is a barrier to the habitability of Mars. *Astrobiology* **2016**, *16*, 427–442, doi:10.1089/ast.2015.1432.
81. Rapin, W.; Ehlmann, B.L.; Dromart, G.; Schieber, J.; Thomas, N.H.; Fischer, W.W.; Fox, V.K.; Stein, N.T.; Nachon, M.; Clark, B.C.; et al. An interval of high salinity in ancient Gale crater lake on Mars. *Nat. Geosci.* **2019**, *12*, 889–895, doi:10.1038/s41561-019-0458-8.
82. Bibring, J.P.; Langevin, Y.; Mustard, J.; Poulet, F.; Arvidson, R.; Gendrin, A.; Gondet, B.; Mangold, N.; Pinet, P.; Forget, F.; et al. Global mineralogical and aqueous Mars history derived from OMEGA/Mars Express data. *Science* **2006**, *312*, 400–404, doi:10.1126/science.1108806.
83. Poulet, F.; Bibring, J.-P.; Mustard, J.; Gendrin, A.; Mangold, N.; Langevin, Y.; Arvidson, R.; Gondet, B.; Gomez, C. Phyllosilicates on Mars and implications for early Martian climate. *Nature* **2005**, *438*, 623–627.
84. Fairén, A.G.; Schulze-Makuch, D.; Rodríguez, A.P.; Fink, W.; Davila, A.F.; Uceda, E.R.; Furfaro, R.; Amils, R.; McKay, C.P. Evidence for Amazonian acidic liquid water on Mars—A reinterpretation of MER mission results. *Planet. Space Sci.* **2009**, *57*, 276–287.
85. Viollier, E.; Inglett, P.W.; Hunter, K.; Roychoudhury, A.N.; Van Cappellen, P. The ferrozine method revisited: Fe(II)/Fe(III) determination in natural waters. *Appl. Geochem.* **2000**, *15*, 785–790, doi:10.1016/s0883-2927(99)00097-9.
86. Delany, J.; Lundeen, S.R. *The LLNL Thermochemical Database*; Report UCRL-21658; Lawrence Livermore National Laboratory: Livermore, CA, USA, 1990; p. 150.
87. Catalano, J.G. Thermodynamic and mass balance constraints on iron-bearing phyllosilicate formation and alteration pathways on early Mars. *J. Geophys. Res. Planets* **2013**, *118*, 2124–2136, doi:10.1002/jgre.20161.
88. Doebelin, N.; Kleeberg, R. Profex: A graphical user interface for the Rietveld refinement program BGMN. *J. Appl. Crystallogr.* **2015**, *48*, 1573–1580, doi:10.1107/s1600576715014685.
89. Bergmann, J.; Friedel, P.; Kleeberg, R. BGMN—A new fundamental parameters based Rietveld program for laboratory X-ray sources, its use in quantitative analysis and structure investigations. *CPD Newslett.* **1998**, *20*, 5–8.
90. Detournay, P.J.; Derie, R.; Ghodsi, M. Etude de l'oxydation par aeration de $Fe(OH)_2$ en milieu chlorure. *Z. Anorg. Allg. Chem.* **1976**, *427*, 265–273, doi:10.1002/zaac.654270311.
91. Taylor, R. Influence of chloride on the formation of iron oxides from Fe (II) chloride. II. Effect of [Cl] on the formation of lepidocrocite and its crystallinity. *Clays Clay Miner.* **1984**, *32*, 175–180, doi:10.1346/CCMN.1984.0320303.
92. Bibi, I.; Singh, B.; Silvester, E. Akaganéite (β-FeOOH) precipitation in inland acid sulfate soils of south-western New South Wales (NSW), Australia. *Geochim. Cosmochim. Acta* **2011**, *75*, 6429–6438, doi:10.1016/j.gca.2011.08.019.
93. Peretyazhko, T.S.; Pan, M.J.; Ming, D.W.; Rampe, E.B.; Morris, R.V.; Agresti, D.G. Reaction of akaganeite with Mars-relevant anions. *ACS Earth Space Chem.* **2019**, *3*, 314–323, doi:10.1021/acsearthspacechem.8b00173.
94. Rémazeilles, C.; Refait, P. On the formation of β-FeOOH (akaganéite) in chloride-containing environments. *Corros. Sci.* **2007**, *49*, 844–857, doi:10.1016/j.corsci.2006.06.003.
95. Ståhl, K.; Nielsen, K.; Jiang, J.Z.; Lebech, B.; Hanson, J.C.; Norby, P.; van Lanschot, J. On the akaganeite crystal structure, phase transformations and possible role in post-excavational corrosion of iron artifacts. *Corros. Sci.* **2003**, *45*, 2563–2575, doi:10.1016/s0010-938x(03)00078-7.
96. Tosca, N.J.; McLennan, S.M.; Dyar, M.D.; Sklute, E.C.; Michel, F.M. Fe oxidation processes at Meridiani Planum and implications for secondary Fe mineralogy on Mars. *J. Geophys. Res. Planets* **2008**, *113*, E05005, doi:10.1029/2007je003019.
97. Regenspurg, S.; Brand, A.; Peiffer, S. Formation and stability of schwertmannite in acidic mining lakes. *Geochim. Cosmochim. Acta* **2004**, *68*, 1185–1197, doi:10.1016/j.gca.2003.07.015.
98. Caraballo, M.A.; Rimstidt, J.D.; Macías, F.; Nieto, J.M.; Hochella, M.F., Jr. Metastability, nanocrystallinity and pseudo-solid solution effects on the understanding of schwertmannite solubility. *Chem. Geol.* **2013**, *360*, 22–31, doi:10.1016/j.chemgeo.2013.09.023.

99. Acero, P.; Ayora, C.; Torrentó, C.; Nieto, J.-M. The behavior of trace elements during schwertmannite precipitation and subsequent transformation into goethite and jarosite. *Geochim. Cosmochim. Acta* **2006**, *70*, 4130–4139, doi:10.1016/j.gca.2006.06.1367.
100. Schwertmann, U.; Carlson, L. The pH-dependent transformation of schwertmannite to goethite at 25 °C. *Clay Miner.* **2005**, *40*, 63–66, doi:10.1180/0009855054010155.
101. Burton, E.D.; Bush, R.T.; Sullivan, L.A.; Mitchell, D.R. Schwertmannite transformation to goethite via the Fe (II) pathway: Reaction rates and implications for iron–sulfide formation. *Geochim. Cosmochim. Acta* **2008**, *72*, 4551–4564, doi:10.1016/j.gca.2008.06.019.
102. Kumpulainen, S.; Räisänen, M.-L.; Von der Kammer, F.; Hofmann, T. Ageing of synthetic and natural schwertmannites at pH 2–8. *Clay Miner.* **2008**, *43*, 437–448, doi:10.1180/claymin.2008.043.3.08.
103. Bigham, J.; Schwertmann, U.; Traina, S.; Winland, R.; Wolf, M. Schwertmannite and the chemical modeling of iron in acid sulfate waters. *Geochim. Cosmochim. Acta* **1996**, *60*, 2111–2121, doi:10.1016/0016-7037(96)00091-9.
104. Peretyazhko, T.; Zachara, J.M.; Boily, J.-F.; Xia, Y.; Gassman, P.L.; Arey, B.W.; Burgos, W.D. Mineralogical transformations controlling acid mine drainage chemistry. *Chem. Geol.* **2009**, *262*, 169–178, doi:10.1016/j.chemgeo.2009.01.017.
105. Sidhu, P.S.; Gilkes, R.J.; Cornell, R.M.; Posner, A.M.; Quirk, J.P. Dissolution of iron-oxides and oxyhydroxides in hydrochloric and perchloric acids. *Clays Clay Miner.* **1981**, *29*, 269–276, doi:10.1346/ccmn.1981.0290404.
106. Sweeton, F.; Baes, C., Jr. The solubility of magnetite and hydrolysis of ferrous ion in aqueous solutions at elevated temperatures. *J. Chem. Thermodyn.* **1970**, *2*, 479–500.
107. Salmimies, R.; Mannila, M.; Kallas, J.; Häkkinen, A. Acidic dissolution of magnetite: Experimental study on the effects of acid concentration and temperature. *Clays Clay Miner.* **2011**, *59*, 136–146, doi:10.1346/CCMN.2011.0590203.
108. Salmimies, R.; Vehmaanperä, P.; Häkkinen, A. Acidic dissolution of magnetite in mixtures of oxalic and sulfuric acid. *Hydrometallurgy* **2016**, *163*, 91–98, doi:10.1016/j.hydromet.2016.03.011.
109. Murad, E.; Cashion, J. Iron oxides. In *Mössbauer Spectroscopy of Environmental Materials and Their Industrial Utilization*; Springer: Boston, MA, USA, 2004; pp. 159–188.
110. Jolivet, J.-P.; Tronc, E. Interfacial electron transfer in colloidal spinel iron oxide. Conversion of Fe_3O_4-γFe_2O_3 in aqueous medium. *J. Colloid Interface Sci.* **1988**, *125*, 688–701, doi:10.1016/0021-9797(88)90036-7.
111. Schwertmann, U.; Cornell, R.M. *Iron Oxides in the Laboratory: Preparation and Characterization*, 2nd ed.; John Wiley & Sons: Weinheim, Germany, 2008.
112. Burns, R.G.; Fisher, D.S. Rates of oxidative weathering on the surface of Mars. *J. Geophys. Res. Planets* **1993**, *98*, 3365–3372, doi:10.1029/92je02055.
113. Schwertmann, U.; Stanjek, H.; Becher, H.H. Long-term in vitro transformation of 2-line ferrihydrite to goethite/hematite at 4, 10, 15 and 25 °C. *Clay Miner.* **2004**, *39*, 433–438, doi:10.1180/0009855043940145.
114. Schwertmann, U.; Friedl, J.; Stanjek, H. From Fe(III) ions to ferrihydrite and then to hematite. *J. Colloid Interface Sci.* **1999**, *209*, 215–223, doi:10.1006/jcis.1998.5899.
115. Schwertmann, U.; Friedl, J.; Stanjek, H.; Schulze, D.G. The effect of Al on Fe oxides. XIX. Formation of Al-substituted hematite from ferrihydrite at 25 °C and pH 4 to 7. *Clays Clay Miner.* **2000**, *48*, 159–172.
116. Schwertmann, U.; Friedl, J.; Stanjek, H.; Schulze, D.G. The effect of clay minerals on the formation of goethite and hematite from ferrihydrite after 16 years' ageing at 25 °C and pH 4–7. *Clay Miner.* **2000**, *35*, 613–623, doi:10.1180/000985500547034.
117. Fischer, W.R.; Schwertmann, U. Formation of hematite from amorphous iron(III) hydroxide. *Clays Clay Miner.* **1975**, *23*, 33–37, doi:10.1346/ccmn.1975.0230105.
118. Schwertmann, U.; Murad, E. Effect of pH on the formation of goethite and hematite from ferrihydrite. *Clays Clay Miner.* **1983**, *31*, 277–284, doi:10.1346/ccmn.1983.0310405.
119. Jiang, Z.; Liu, Q.; Roberts, A.P.; Barrón, V.; Torrent, J.; Zhang, Q. A new model for transformation of ferrihydrite to hematite in soils and sediments. *Geology* **2018**, *46*, 987–990.
120. Tosca, N.J.; Knoll, A.H. Juvenile chemical sediments and the long term persistence of water at the surface of Mars. *Earth Planet. Sci. Lett.* **2009**, *286*, 379–386.
121. Cornell, R.; Giovanoli, R. Transformation of akaganeite into goethite and hematite in alkaline media. *Clays Clay Miner.* **1990**, *38*, 469–476.

122. Goñi-Elizalde, S.; Garcia-Clavel, M.E.; Tejedor-Tejedor, M.I. Mechanism of akaganeite-hematite transformation via solution. *React. Solids* **1987**, *3*, 139–154.
123. Frandsen, C.; Legg, B.A.; Comolli, L.R.; Zhang, H.; Gilbert, B.; Johnson, E.; Banfield, J.F. Aggregation-induced growth and transformation of β-FeOOH nanorods to micron-sized α-Fe_2O_3 spindles. *CrystEngComm* **2014**, *16*, 1451–1458.
124. Peterson, K.M.; Heaney, P.J.; Post, J.E. Evolution in the structure of akaganeite and hematite during hydrothermal growth: An in situ synchrotron X-ray diffraction analysis. *Powder Diffr.* **2018**, *33*, 287–297.
125. Gendrin, A.; Mangold, N.; Bibring, J.P.; Langevin, Y.; Gondet, B.; Poulet, F.; Bonello, G.; Quantin, C.; Mustard, J.; Arvidson, R.; et al. Sulfates in Martian layered terrains: The OMEGA/Mars Express view. *Science* **2005**, *307*, 1587–1591, doi:10.1126/science.1109087.
126. Bibring, J.P.; Langevin, Y.; Gendrin, A.; Gondet, B.; Poulet, F.; Berthe, M.; Soufflot, A.; Arvidson, R.; Mangold, N.; Mustard, J.; et al. Mars surface diversity as revealed by the OMEGA/Mars Express observations. *Science* **2005**, *307*, 1576–1581, doi:10.1126/science.1108806.
127. Glotch, T.D.; Rogers, A.D. Evidence for aqueous deposition of hematite- and sulfate-rich light-toned layered deposits in Aureum and Iani Chaos, Mars. *J. Geophys. Res. Planets* **2007**, *112*, E06001, doi:10.1029/2006je002863.
128. Fernández-Remolar, D.C.; Morris, R.V.; Gruener, J.E.; Amils, R.; Knoll, A.H. The Río Tinto Basin, Spain: Mineralogy, sedimentary geobiology, and implications for interpretation of outcrop rocks at Meridiani Planum, Mars. *Earth Planet. Sci. Lett.* **2005**, *240*, 149–167, doi:10.1016/j.epsl.2005.09.043.
129. Archer, P.D.; Franz, H.B.; Sutter, B.; Arevalo, R.D.; Coll, P.; Eigenbrode, J.L.; Glavin, D.P.; Jones, J.J.; Leshin, L.A.; Mahaffy, P.R. Abundances and implications of volatile-bearing species from evolved gas analysis of the Rocknest aeolian deposit, Gale Crater, Mars. *J. Geophys. Res. Planets* **2014**, *119*, 237–254, doi:10.1002/2013JE004493.
130. David, G.; Cousin, A.; Forni, O.; Meslin, P.Y.; Dehouck, E.; Mangold, N.; L'Haridon, J.; Rapin, W.; Gasnault, O.; Johnson, J. Analyses of high-iron sedimentary bedrock and diagenetic features observed with ChemCam at Vera Rubin ridge, Gale crater, Mars: Calibration and characterization. *J. Geophys. Res. Planets* **2020**, doi:10.1029/2019JE006314.
131. Grotzinger, J.P.; Sumner, D.Y.; Kah, L.; Stack, K.; Gupta, S.; Edgar, L.; Rubin, D.; Lewis, K.; Schieber, J.; Mangold, N. A habitable fluvio-lacustrine environment at Yellowknife Bay, Gale Crater, Mars. *Science* **2014**, *343*, 1242777.